



UNIVERSITY OF LEEDS

This is a repository copy of *Ultrafast terahertz detectors based on three-dimensional meta-atoms*.

White Rose Research Online URL for this paper:
<http://eprints.whiterose.ac.uk/125220/>

Version: Supplemental Material

Article:

Paulillo, B, Pirotta, S, Nong, H et al. (8 more authors) (2017) Ultrafast terahertz detectors based on three-dimensional meta-atoms. *Optica*, 4 (12). pp. 1451-1456. ISSN 2334-2536

<https://doi.org/10.1364/OPTICA.4.001451>

(c) 2017, Optical Society of America. This is an author produced version of a paper published in *Optica*. One print or electronic copy may be made for personal use only. Systematic reproduction and distribution, duplication of any material in this paper for a fee or for commercial purposes, or modifications of the content of this paper are prohibited.

Reuse

Items deposited in White Rose Research Online are protected by copyright, with all rights reserved unless indicated otherwise. They may be downloaded and/or printed for private study, or other acts as permitted by national copyright laws. The publisher or other rights holders may allow further reproduction and re-use of the full text version. This is indicated by the licence information on the White Rose Research Online record for the item.

Takedown

If you consider content in White Rose Research Online to be in breach of UK law, please notify us by emailing eprints@whiterose.ac.uk including the URL of the record and the reason for the withdrawal request.



eprints@whiterose.ac.uk
<https://eprints.whiterose.ac.uk/>

Electromagnetic Simulations

The electromagnetic simulations of the structure (array geometry) shown in Fig. 2 have been performed with a finite elements solver (Comsol Multiphysics). The impinging planewave is x-polarized, so that the magnetic field (y-direction, see Fig. inset) couples with the loop antenna magnetic dipole. To mimic the experimental array configuration, a $25 \times 15 \mu\text{m}^2$ unit cell is considered. The metal domains are modelled with a dispersive Drude permittivity¹, the patterned ground plane is presumed to be a perfect-metal boundary, and the substrate is undoped GaAs with a permittivity given by the Lorentz model². The 1.5- μm -thick GaAs filling the MSM capacitor is modelled with the Drude-Lorentz model including a volume doping of 10^{15}cm^{-3} to compute dissipation in the active core. The MSM capacitor diameter is 4 μm , and the antenna total length is $\approx 10 \mu\text{m}$, to set the LC resonance around 3 THz³. In order to clarify the polarisation response of the meta-atoms array Figure S1 shows the simulated reflectivity spectra for both polarizations of impinging light: the magnetic field is parallel and orthogonal to the antenna as sketched in the inset. The colour scheme is the same as in Figure 3 (a) of the main text for coherence. In the same picture we also highlight the role of the gold ground plane (GP) etching in the optical response of the array: a clear absorption around 3 THz is present in the case of continuous GP with the correct polarization (H orthogonal to the antenna, red curves): this is the pure RLC resonance. By opening the GP, as explained in the main text, new modes arise in the spectrum that can then couple to the RLC mode giving a broadening of the absorption region: the polarization dependence is preserved.

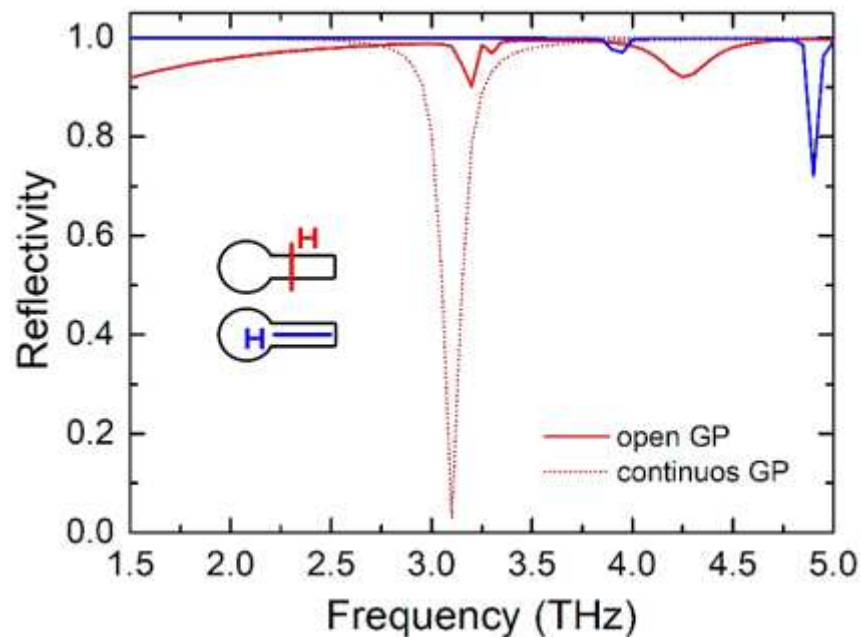


Figure S1. Simulated reflectivity spectra of an array of meta-atoms illuminated by normally incident THz radiation for both polarizations shown in the inset. Dotted red line: the ground plane is continuous (continuous GP). Full red line: the ground plane is patterned for contacts (open GP) as explained in the main text, and the polarization couples to the loop antenna. Full blue line: the ground plane is patterned for contacts, but the polarization does not couple to the loop antenna.

Sample Fabrication

The QWIP GaAs/AlGaAs epitaxy (grown on a GaAs substrate) is Ti/Au coated together with a second GaAs wafer holder. The sample carrier is glued on the holder via thermocompressive Au-Au bonding. The original GaAs substrate is then removed via mechano-chemical polishing. Once the GaAs/AlGaAs epitaxy is uncovered, MSM patches are defined via chlorine-based ICP-RIE dry etch using a metal mask obtained with standard contact photolithography and lift-off. Later, the metal ground plane is ion beam etched using a photoresist mask. The ground plane patterning is devised to obtain separate contact domains either for a single pixel or an array of devices. Finally, to define the suspended loop antenna we used a two-step process: first a scaffold for sustaining the antenna is formed using a positive photoresist (S1818); then the metal stripe constituting the antenna is defined using a negative photoresist (AZ5214) and lift-off. Back-end process consists in a gold evaporation on the sample backside (to improve thermal contact) and sample cutting via micro-dicing with a diamond blade.

Active Region Characterisation in Mesa Geometry

To verify that the QWIP used as active region in this work structure (epitaxy L1258) provides the intersubband absorption requested by design as a first step we verified its optical response in a standard mesa geometry. The heterostructure has been processed in square mesas of 220 or 440 μm side using the standard mesa fabrication protocol: i) wet etching of the active region; ii) definition of the bottom ohmic contact (annealed Ni/Ge/ Au/Ni/Au); definition of the ohmic top contact (annealed Pd/Ge + Ti/Au). The fabricated sample has been tested in a 45 deg substrate-coupling geometry as sketched in the inset of Figure S2(a). The experimental setup for photocurrent spectra measurements, both for mesas and meta-atom detectors, is shown in Figure S2(b). The light from the THz source (internal FTIR broadband source or external THz QCL) is focused by a TPX lens on the sample, mounted in a LHe continuous-flow cryostat. The photocurrent generated in the active region is then amplified by a trans-impedance amplifier (TIA) and sent back to the FTIR to recover the photocurrent spectrum. Note: a lock-in amplifier (LIA) can be used to maximize the signal on the detector by chopping the incident beam, whereas it is not needed to acquire the spectrum in rapid scan modulation.

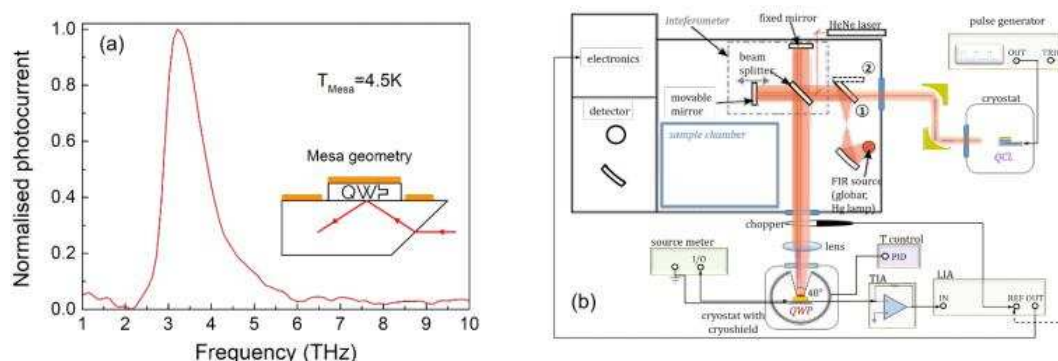


Figure S2.

(a) Photocurrent spectrum of L1258 QWIP processed in a square mesa configuration.

(b) Experimental setup for photocurrent spectra measurements. Two configurations are possible depending on the position of the movable mirror:

(1) internal broadband source (Glohar or discharge Hg lamp) or

(2) external source, typically a QCL laser. TIA=trans-impedance amplifier, LIA=lock-in amplifier.

Background limited infrared performance

We directly measure the current-voltage characteristic from the samples mounted on the cryostat using a Keithley 2636A source meter. Two configurations have been explored in order to extract the background limited infrared performance temperature (TBLIP)⁴ as well as the responsivity of our detectors: the left panel in Figure S3(a) shows the detector seeing a 300K background (materialized by a 300 K blackbody placed in front of the cryostat TPX window) from a finite aperture in the cryoshield (field of view =24 deg). In the right panel of Figure S3(a) the cryoshield is completely wrapped with metal; this configuration allows the measurement of the dark current. Figure S3(b) shows a typical I-V curve measured at 4.5K under background illumination (red) and dark condition (black) for a single pixel device, showing currents well below 1nA in the typical applied bias range (+/- 50mV). By measuring the I-V curves in both conditions for different sample temperatures we can estimate the BLIP temperature from the ratio I_{BB}/I_{Dark} as reported in Figure S3(c) for the 300 pixel array and Figure S3(d) for the single pixel. Both graphs show a TBLIP of about 7-8K, in accordance with the literature values for this design.

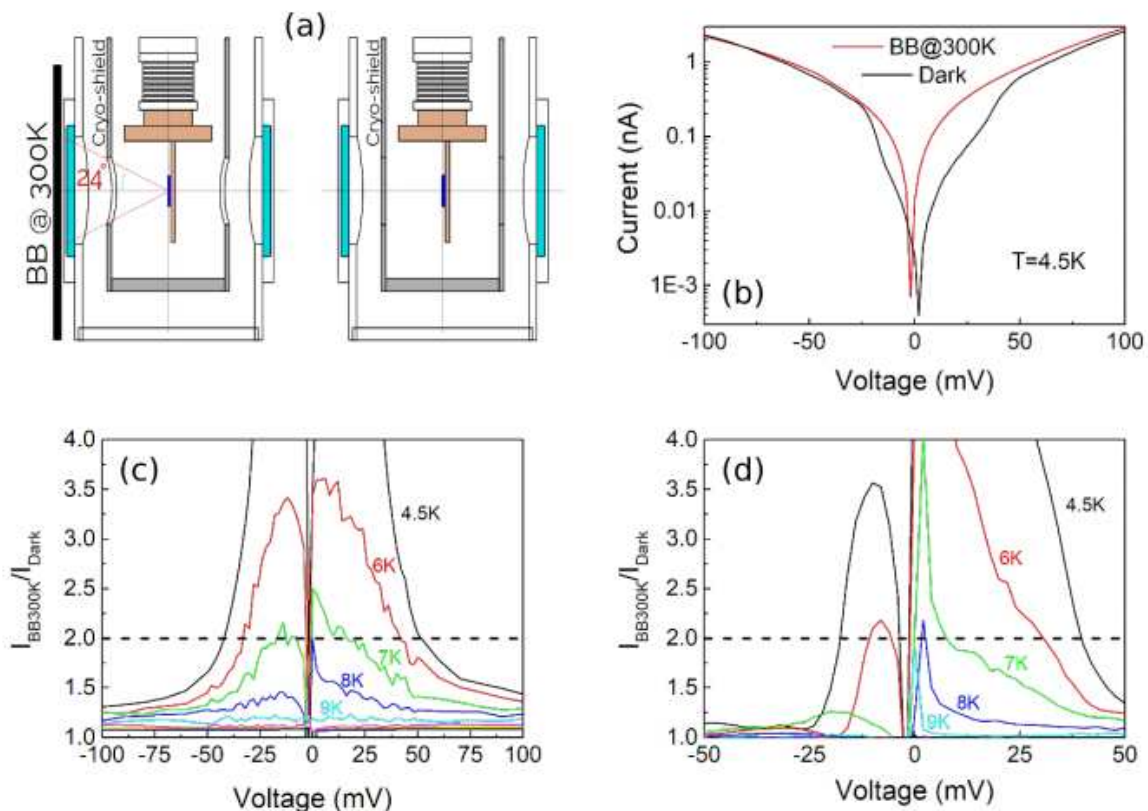


Figure S3.

(a) Setup for electrical characterization: (left) the sample sees a black body @ 300K and (right) the cryoshield is entirely closed around the sample.

(b) Current-voltage curves under dark condition (black solid line) and under illumination from a 300K black body (red solid line) for a single pixel device.

(c) Ratio I_{BB}/I_{Dark} for the QWIP array at increasing temperature from 4.5K to 10K.

(d) Ratio I_{BB}/I_{Dark} for the single pixel QWIP at increasing temperature from 4.5K to 10K. The BLIP temperature is around 7-8K in both cases.

Estimation of the Background Radiant Power Impinging on the Detector

The radiant power impinging on the detector depends on the projected solid angle through which the detector observes the source. In the case of a round aperture centred over the detector (in our experiments, a cryo-shield with FOV $\theta=48^\circ$) the projected solid angle⁶ is $\Omega_p = \pi \sin^2(\theta/2) = 0.519$ sr. The radiance L of the 300 K blackbody can be obtained by integrating Planck's law over the detector spectral sensitivity window (2.69-3.23 THz, from mesa characterisation) which yields $L=0.34$ W/(m²sr). Finally, given the array detector area $A_d=310 \times 360 \mu\text{m}^2$, the power seen by the detector is estimated as $I \approx L A_d \Omega_p \approx 20$ nW.

S11 Data vs Model (linear plot)

In Figure S4 the linear representations of the experimental S11 parameters (magnitude and phase) together with the equivalent circuit model – both previously represented on the Smith plot in Figure 5 as normalized impedances z – are shown.

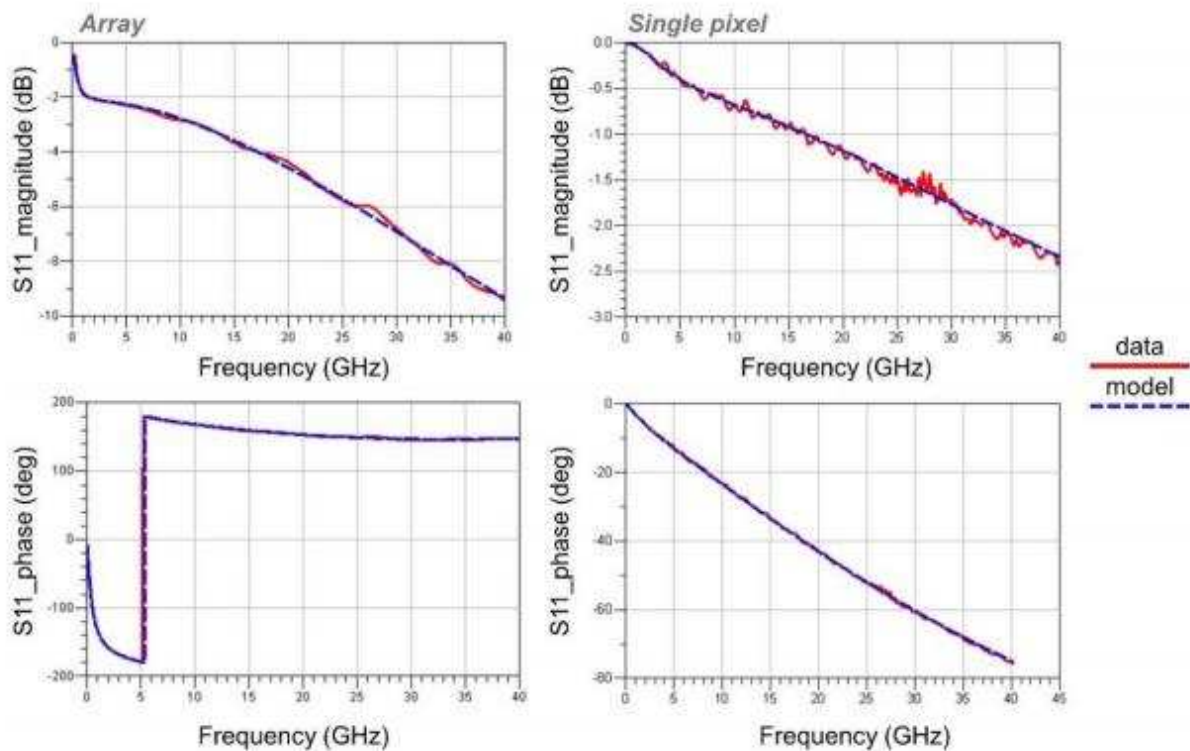


Figure S4. Linear plot of the S11 parameters (magnitude and phase, data vs model) shown in Figure 5 for an array(left) and a single pixel (right).

References

1. Ordal, M. A., Bell, R. J., Alexander, R. W., Long, L. L. & Query, M. R. Optical properties of fourteen metals in the infrared and far infrared: Al, Co, Cu, Au, Fe, Pb, Mo, Ni, Pd, Pt, Ag, Ti, V, and W. *Appl. Opt.* 24, 4493– 4499 (1985).
2. Palik, E. D. *Handbook of Optical Constants of Solids II.* (Academic Press, 1991).
3. Paulillo, B. et al. Circuit-tunable sub-wavelength THz resonators: hybridizing optical cavities and loop antennas. *Opt. Express* 22, 21302 (2014).
4. Rosencher, E. & Vinter, B. *Optoelectronics.* (Cambridge University Press, 2002).
5. Luo, H., Liu, H. C., Song, C. Y. & Wasilewski, Z. R. Background-limited terahertz quantum-well photodetector. *Appl. Phys. Lett.* 86, 1–3 (2005).
6. Vincent, J. D., Vampola, J., Hodges, S., Pierce, G. & Stegall, M. *Fundamentals of Infrared and Visible Detector Operation and Testing.* (Wiley, 2015).